Check for updates

Anderson-type polyoxometalate-based metal–organic framework as an efficient heterogeneous catalyst for selective oxidation of benzylic C–H bonds†

Hong-Ru Tan,[a] Xiang Zhou,[b] Tengfei Gong,[c] Hanqi You,[a] Qi Zheng, [iD][b] Sheng-Yin Zhao [iD] *[a] and Weimin Xuan [iD] *[a]

Oxidative transformation of benzylic C–H bonds into functional carbonyl groups under mild conditions represents an efficient method for the synthesis of aromatic carboxylic acids and ketones. Here we report a high-efficiency catalyst system constructed from an Anderson-type polyoxometalate-based metal–Organic framework (**POMOF-1**) and *N*-hydroxyphthalimide (NHPI) for selective oxidation of methylarenes and alkylarenes under 1 atm O$_2$ atmosphere. **POMOF-1** exerted a synergistic effect originating from the well-aligned Anderson {CrMo$_6$} clusters and Cu centers within the framework, and this entailed good cooperation with NHPI to catalyze the selective oxidation. Accordingly, the reactions exhibit good tolerance and chemical selectivity for a wide range of substrates bearing diverse substituent groups, and the corresponding carboxylic acids and ketones were harvested in good yields under mild conditions. Mechanism study reveals that **POMOF-1** worked synergistically with NPHI to activate the benzylic C–H bonds of substrates, which are sequentially oxidized by oxygen and HOO$^•$ to give rise to the products. This work may pave a way to design high-efficiency catalysts by integration of polyoxometalate-based materials with NPHI for challenging C–H activation.

Introduction

The selective oxidation of alkylaromatic hydrocarbons is of great fundamental and practical importance to manufacture value-added alcohols, aldehydes, ketones and carboxylic acids.[1–5] Evolving from conventional Cr(VI) and Mn(VII)-based reagents, the application of air or molecular oxygen as a green oxidant has aroused constant attention.[6–11] The most impressive demonstration of this methodology includes the industrial production of benzoic acid using a Co/Mn/Br/AcOH system *via* selective oxidation of toluene with O$_2$, which manifests the high-efficiency by combination of catalytic metal centers with bromide as a promoter.[12–16] However, the system suffers from strong corrosion owing to the presence of bromide ions and intermediate hydroperoxides in acidic medium.[17] In this

context, metal/*N*-hydroxyphthalimide (NHPI) systems such as Co(OAc)$_2$/NHPI and Co(OAc)$_2$/Mn(OAc)$_2$/NHPI have been developed as highly effective alternatives that facilitate oxidative conversion of alkylaromatic hydrocarbons into benzoic acid and terephthalic acid under more environmentally benign conditions.[18–23] In view of the high-efficiency of the above systems, combination of solid supports containing metal sites with NHPI has emerged as a versatile approach to build effective catalyst systems.[22,24,25] The confined surfaces and well-defined active sites of the solid support can on one hand improve the activity and stability of NHPI, while on the other hand promote the catalysis in a cooperative manner with NHPI absorbed on the surface.[26,27] As such, the activity and selectivity can be modulated so that higher catalysis efficiency is achieved as compared with the homogeneous counterparts. For example, employing metal–organic frameworks (MOFs) as porous platform to accommodate NHPI, a variety of oxidative transformations were catalyzed by MOF/NHPI systems, including oxidative coupling of benzylamines, aerobic oxidation of alkanes and alkenes, and selective oxidation of benzylic C–H bonds.[28–32] In all these cases, the integrated catalyst systems showed catalytic performance superior to the homogeneous mixture of metal salts and NHPI.

Polyoxometalates (POMs), a class of versatile and discrete anionic metal oxides with unique properties, have been applied in catalysis, materials science and medicine.[33–38] POMs have

[a]State Key Laboratory for Modification of Chemical Fibers and Polymer Materials, College of Chemistry and Chemical Engineering, Donghua University, Shanghai 201620, P. R. China. E-mail: syzhao8@dhu.edu.cn; weiminxuan@dhu.edu.cn

[b]State Key Laboratory for Modification of Chemical Fibers and Polymer Materials, College of Materials Science and Engineering, Donghua University, Shanghai 201620, P. R. China. E-mail: qi.zheng@dhu.edu.cn

[c]Jiaxing Jiayuan Inspection Technology Service Co., Ltd, Building 2, No. 1403, Hongbo Road, Economic and Technological Development Zone, Jiaxing City, Zhejiang Province, P. R. China

† Electronic supplementary information (ESI) available. CCDC 2300360. For ESI and crystallographic data in CIF or other electronic format see DOI: https://doi.org/10.1039/d3ra07120k
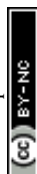
been well established as high-efficiency catalysts for oxidative transformation due to their inherent strong oxidizing ability, reversible multi-electron redox property, and high resistance to oxidative decomposition.[39–44] Integrated with NHPI, POM clusters such as $Mo_{72}V_{30}$ can facilely catalyze the oxidation of benzylic alcohols and hydrocarbons to corresponding aldehydes or ketones.[45,46] Going beyond the homogeneous system, Installation of Cu-containing POM clusters within crystalline porous all-inorganic framework, the resulted heterogeneous catalyst can cooperate well with NHPI to promote biomimetic aerobic oxidation of aliphatic alcohols into carboxylic acids.[47] Alternatively, employing Cu-porphyrin functionalized MOF as solid support to work synergistically with POM cluster and NHPI as co-catalyst platform has also furnished the production of phenylketones *via* aerobic oxidation of arylalkanes.[48] As demonstrated above, combination of NHPI with catalytic transition metal sites and POM clusters which are incorporated within robust frameworks facilitates the catalytic oxidation. Along with these lines, we postulate that direct assembly of metal nodes, POM cluster and organic linkers to build polyoxometalate-based metal–organic frameworks (POMOFs) can offer multifunctional supports to function with NHPI for other advanced oxidative transformations.

Herein, we reported that the design and synthesis of a 2D POMOF $H_2[Cu_4(OH)_2(H_2O)_7L_2(CrMo_6)_2]\cdot 6H_2O$ (**POMOF-1**, **L** = 1,3-di-(1,2,4-triazol-4-yl)benzene, $CrMo_6 = [CrMo_6O_{18}(OH)_5]$ for selective oxidation of benzylic C–H bonds to carbonyl compounds (Scheme 1). **POMOF-1** is constructed from Anderson-type POM $Na_3[CrMo_6O_{18}(OH)_5]$, **L** and Cu^{2+}, and features a 2D layered structure *via* the connection of $CrMo_6$ clusters and 1D metal–organic chains built from $\{Cu_4O_3\}$ units and **L**. The presence of catalytically active POM clusters and abundant Cu^{2+} sites make **POMOF-1** an excellent platform for catalytic oxidation of benzylic C–H bonds with NHPI as co-catalyst. Owing to the synergistic effect of functional components, **POMOF-1** showed high activity and selectivity towards the oxidative transformation of methylarenes into aryl carboxylic acids. In particular, dimethyl and trimethyl-substituted substrates can also be selectively and facilely converted into aromatic monocarboxylic acid. Besides, the high-efficiency system can further be applied for oxidation of alkylarenes to afford ketones in good yields. **POMOF-1** is stable and could be recycled for five times without noticeable loss of catalytic activity.

Experimental

Unless otherwise noted, all the materials were purchased from commercial suppliers and used without further purification. **L** and $Na_3[CrMo_6O_{18}(OH)_6]$ are prepared according to literature with some modifications. The detailed synthetic process and characterization is described in ESI.†

Preparation of POMOF-1

$CuCl_2\cdot 2H_2O$ (5.38 mg, 0.04 mmol), **L** (4.24 mg, 0.02 mmol) and $Na_3[CrMo_6O_{18}(OH)_6]$ (17.96 mg 0.015 mmol) were added into
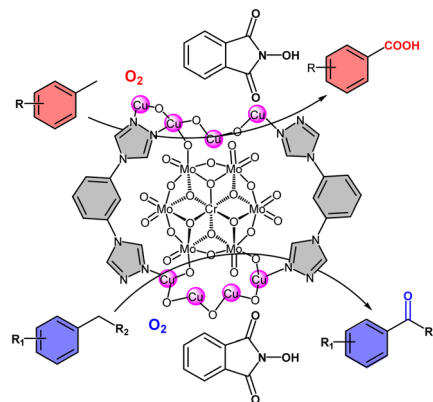
Scheme 1 Catalytic oxidation of benzylic C–H bonds promoted by **POMOF-1** and NHPI.

H_2O (5 mL). The solution was stirred and pH was adjusted to 3.6 by 1 M HCl. Then the mixture was heated in a Teflon-lined stainless steel reactor at 140 °C for 3 days. After cooling to room temperature, green bulk crystals were obtained by filtration and washed with DMSO, H_2O, EtOH and Et_2O. Yield: 14.3 mg. 32.4% based on Cr. Elemental analysis for **POMOF-1** $(H_2[Cu_4(OH)_2(H_2O)_7L_2(CrMo_6)_2]\cdot 6H_2O)$: C 8.16%, H 1.56%, N 5.71%, Cr 3.54%, Mo 39.16%, Cu 8.65%; found: C 8.01%, H 1.77%, N 5.62%, Cr 3.56%, Mo 39.03%, Cu 8.77%. FT-IR (cm^{-1}): 3369, 2960, 2872, 1637, 1479, 1381, 1116, 1026, 935, 911, 894, 638, 563.

General methods for oxidation reaction of methylarenes

POMOF-1 (0.1 mol%), NHPI (0.04 mmol), methylarenes **1** (0.2 mmol) and CH_3CN (1 mL) were added into seal tube, which was subsequently charged with 1 atm O_2. Then the reaction was heated at 85 °C and kept stirring for 24 h. The reactor was cooled to room temperature, the catalyst was centrifuged and the supernatant was diluted with ethyl acetate. The conversion of methylarenes **1** and yields of product aromatic acid **2** were determined by gas chromatography-mass spectrometry (GC-MS) with hexadecane as internal standard. Then, the reaction was quenched with H_2O and extracted with ethyl acetate. Filtering out the insoluble substances, the organic phases were washed with H_2O, and dried over anhydrous Na_2SO_4. The organic phases were filtered and concentrated under reduced pressure and the crude products were purified by silica gel column chromatography (eluent : ethyl acetate–petroleum ether, 1 : 10–5 : 1) to yield the pure products. The products were characterized by ^1H NMR and ^{13}C NMR.

General methods for oxidation reaction of alkylarenes

POMOF-1 (0.1 mol%), alkylarenes **4** (0.2 mmol) and CH_3CN (1 mL) were added into seal tube, which was subsequently charged with 1 atm O_2. Then the reaction was heated at 85 °C and kept stirring for 6 h. The reactor was cooled to room temperature, the catalyst was centrifuged and the supernatant was diluted with ethyl acetate. The conversion of alkylarenes **4** and yields of

product aromatic ketones **5** were determined by gas chromatography-mass spectrometry (GC-MS) with hexadecane as internal standard. Then, the reaction was quenched with H_2O and extracted with ethyl acetate. Filtering out the insoluble substances, the organic phases were washed with H_2O, and dried over anhydrous Na_2SO_4. The organic phases were filtered and concentrated under reduced pressure and the crude products were purified by silica gel column chromatography (eluent : ethyl acetate–petroleum ether, 1 : 100–500) to yield the pure products. The products were characterized by ^{1}H NMR and ^{13}C NMR.

Results and discussion

Crystal structure of POMOF-1

Hydrothermal reaction of **L**, $CuCl_2$ and $Na_3[CrMo_6O_{18}(OH)_6]$ in acidified aqueous solution at 140 °C resulted in green bulk crystals of $H_2[Cu_4(OH)_2(H_2O)_{7}L_2\{CrMo_6\}_2]\cdot6H_2O$ (**POMOF-1**). The crystallographic data and structural refinement parameters are summarized in Table S1.† The Single-crystal X-ray diffraction structure analysis reveals that **POMOF-1** crystallizes in the triclinic $P\bar{1}$ space group. The asymmetric unit of **POMOF-1** consists of four Cu^{2+}, two **L**, two $\{CrMo_6\}$ clusters, two μ_3-OH atoms and seven coordination water (Fig. 1a). With connection of two μ_3-OH atoms one O from coordination water, the four Cu^{2+} aggregate into a rod-like $\{Cu_4O_3\}$ unit (Fig. 1b). Besides, three triazole moieties alternatively bridge the adjacent Cu centers, further reinforcing the rigidity of $\{Cu_4O_3\}$ unit (Fig. 1b). All the four Cu^{2+} adopt octahedral coordination environments. To fulfill the six coordination sites, along with μ_3-OH atoms

Fig. 1 (a) Asymmetric unit of POMOF-1 (thermal ellipsoids are set as 50% probability level), (b) coordination modes of Cu centers, (c) 1D chain built from $\{Cu_4O_3\}$ and L, (d) 2D layer structure of **POMOF-1**, (e) 3D supramolecular framework formed *via* H-bonds between $\{CrMo_6\}$ from neighbouring 2D layer. $\{CrMo_6\}$ clusters from different layers are represented in yellow and green, respectively, while H-bonds are indicated by dashed two-colored lines in grey and red. (Color scheme: Mo: bright green polyhedron and yellow polyhedron; Cu: cyan; Cr: pink polyhedron; O: red; H: gray; N: light blue; C: black).

and N atoms from μ_2-triazoles, coordination water, terminal O atoms from $\{CrMo_6\}$ clusters and N atoms from **L** occupy the residual coordination sites around Cu_1–Cu_4 (Fig. 1b). With such binding mode, each $\{Cu_4O_3\}$ unit thus connects with four **L** while every **L** links with two $\{Cu_4O_3\}$ units, leading to the formation of 1D metal–organic chain (Fig. 1c). The adjacent 1D chains are further pillared by $\{CrMo_6\}$ clusters and therefore giving rise to a 2D layered structure along *ac* plane (Fig. 1d). Owing to the presence of three μ_3-OH groups on each surface of disk-like $\{CrMo_6\}$ cluster, multiple O···H–O hydrogen bonds (2.6094(1)–2.8806(1) Å) are generated between $\{CrMo_6\}$ clusters lined on neighbouring layers, which assist the layer-by-layer stacking and hence the formation of a 3D supramolecular framework (Fig. 1e). In fact, Anderson-type clusters are well known for the facile formation of strong hydrogen bonding between terminal oxygen atoms and μ_3-OH groups from adjacent clusters in crystalline solids; this has resulted in supramolecular structures from 1D zigzag chain to 3D porous framework.[49,50]

The experimental PXRD pattern of **POMOF-1** agrees well with the simulated data (Fig. S2†), demonstrating its high phase purity. As shown in TGA curve (Fig. S3†), the first weight loss of 7.24% occurs from 50 to 240 °C, which is corresponding to the release of six lattice H_2O molecules and six coordinated water molecules. Afterwards, the organic ligands decompose in the temperature range from 240 to 420 °C with the weight loss of 14.42%. Finally, the collapse of $\{CrMo_6\}$ skeleton happens between 420 and 700 °C. The residue can be attributed to a mixture of CuO, MoO_3 and CrO_3. The FT-IR spectrum of **POMOF-1** clearly shows the characteristic peaks of both **L** and $\{CrMo_6\}$ (Fig. S4†). According to the literature, the bands centered at 935, 911, 894, 638 and 563 cm^{-1} are ascribed to $\nu(Mo=O)$, $\nu(Mo–O–Mo)$, $\nu(Mo–O–Cr)$, $\nu(Mo–O)$, $\nu(Cr–O)$ vibrations of $\{CrMo_6\}$, respectively.[51,52] The peaks at 2960 and 2872 cm^{-1} are corresponding to C–H stretching of the aromatic rings from **L**. Moreover, the characteristic peaks of C=O, C=N, C=C can be clearly identified from 1350 to 1700 cm^{-1}, further confirming the presence of **L**.

Catalytic oxidation of methylarenes by POMOF-1

As an archetypal POM cluster, Anderson POMs are widely used for a variety of catalytic oxidative transformations.[53–56] Meanwhile, as one of the most utilized transition metals, copper is also extensively applied for synthetic organic chemistry.[57–60] Very recently, Copper-based catalyst has showed enzymatic activity for C–H oxidation with NHPI as co-catalyst.[61] By integration of Anderson-type $\{CrMo_6\}$ cluster and $\{Cu_4O_3\}$ unit in the framework of **POMOF-1**, we thus intend to use it as a catalyst for the synthesis of aryl carboxylic acids *via* oxidation of methylarenes.

The investigation was initialized by using toluene (**1a**) as a model substrate (Table 1). The oxidative reaction was carried out under 1 atm O_2 atmosphere in CH_3CN at 85 °C for 24 h using 1 mol% **POMOF-1** as catalyst and 0.2 equivalent NHPI as co-catalyst, benzoic acid (**2a**) can be obtained in a yield of 91% (Table 1, entry 1). Increase of the amount of NHPI afforded
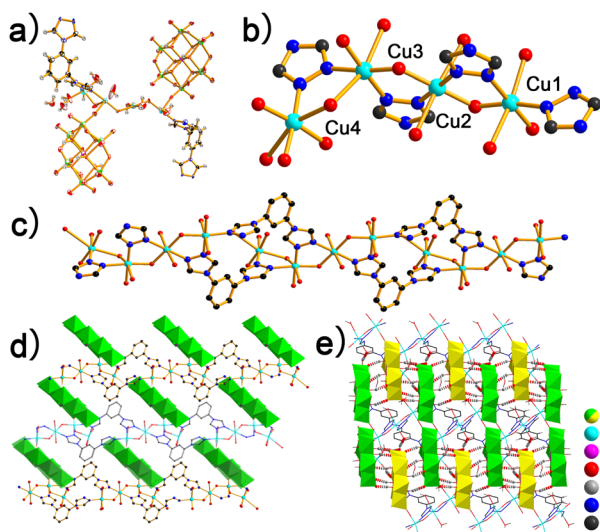
Table 1 Optimization of catalytic oxidation of toluene (**1a**) with POMOF-1[a]

Entry	Add.	Solvent	Yields%
1	0.2 equiv. NHPI	CH₃CN	91
2	0.5 equiv. NHPI	CH₃CN	90
3	0.1 equiv. NHPI	CH₃CN	42
4	0.05 equiv. NHPI	CH₃CN	20
5[b]	0.2 equiv. NHPI	CH₃CN	85
6[c]	0.2 equiv. NHPI	CH₃CN	51
7[d]	0.2 equiv. NHPI	CH₃CN	68
8[e]	0.2 equiv. NHPI	CH₃CN	95
9	0.2 equiv. NHPI	EtOH	Trace
10	0.2 equiv. NHPI	Acetone	18
11	0.2 equiv. NHPI	THF	Trace
12	0.2 equiv. NHPI	DCM	Trace
13	0.2 equiv. NHPI	DMF	Trace
14	0.2 equiv. NHPI	DMSO	Trace
15	None	CH₃CN	Trace
16[f]	0.2 equiv. NHPI	CH₃CN	11
17[g]	0.2 equiv. NHPI	CH₃CN	Trace

[a] Reaction condition: **POMOF-1** (1 mol%), add., solvent (1 mL), toluene **1a** (0.2 mmol) in O₂ atmosphere (1 atm) at 85 °C. Yields were determined by GC-MS and hexadecane as internal standard. [b] Reaction temperature: 95 °C. [c] Reaction temperature: 65 °C. [d] Reaction time: 12 h. [e] Reaction time: 36 h. [f] Under air atmosphere. [g] Under N₂ atmosphere.

Table 2 Scope of oxidation reaction of methylarenes[a]

[a] Reaction condition: **POMOF-1** (1 mol%), NHPI (0.2 equiv.), methylarenes **1** (0.2 mmol) and CH₃CN (1 mL) in O₂ (1 atm) at 85 °C for 24 h. Yields were determined by GC-MS. Hexadecane as internal standard. Values in parentheses are the isolated yields.

similar yield (Table 1, entry 2) while decrease of NHPI to 0.1 and 0.05 equivalent significantly reduced the yield (Table 1, entries 3 and 4). Further optimization of the reaction temperature and time showed 85 °C and 24 h were the optimal conditions (Table 1, entries 5–8). In addition, screening the scope of solvents showed that CH₃CN was the best solvent (Table 1, entries 9–14). Control experiments showed that NHPI and O₂ were essential for the oxidation. As indicated by entry 15, the reaction hardly happened in the absence of NHPI. Performing the catalysis in air atmosphere also led to the production of **2a** albeit in much lower yield (Table 1, entry 16), and the reaction could not proceed in N₂ atmosphere (Table 1, entry 17). After extensive optimization with reaction parameters, it was found that 1.0 mol% **POMOF-1** along with 0.2 equivalent of NHPI in CH₃CN at 85 °C for 24 h was the most optimized reaction condition (Table 1, entry 1).

With the optimized reaction condition, the scope of oxidation reaction of methylarenes was then investigated. As shown in Table 2, the reaction showed good functional group tolerance for a series of substituted toluene in good to excellent yields ranging from 72% to 91% (**2b–2g**). Both the electron-donating methoxy and weak electron-withdrawing bromo/chloro/ester substituted toluene can be facilely converted to corresponding aryl carboxylic acids (**2b–2g**). For strong electron-withdrawing cyan group, targeted products could also be harvested in 70% yield (**2h**). Nitro group severely deactivated the substrate, **2i** was

only acquired in 29% yield. As revealed by the Hammett plot (Fig. S11†), the log of relative reaction rates for *para*-substituted methylarenes correlated very well with Hammett parameter (R^2 = 0.937), affording a ρ value of −0.90, which indicated electron-rich methylarences are favored for oxidative conversion with higher rates.[62,63] Meanwhile, methyl-substituted pyrrole could be smoothly transformed to **2j** in a yield of 62%. Regarding the substrates with bigger size, the linear 4-phenyltoluene and 2-methyl naphthalene can be converted to **2k** and **2l** in a good yield of 76% and 74%, while the conversion of more sterically hindered 1-methyl naphthalene to **2m** was much lower. Next, we pay attention to the selective oxidation of dimethyl and trimethyl-substituted benzene. To our delight, all kinds of xylenes can be selectively oxidized to aromatic monocarboxylic acids in satisfied yields (**2n–2p**). Compared with *m*- and *p*-xylene (**2n, 2o**), the less effective conversion of *o*-xylene may be caused by the steric effect (**2p**). In a similar way, **2q** can be acquired in a yield of 72% from mesitylene. Overall, **POMOF-1** demonstrated general applicability towards a variety of methylarenes.

To confirm the synergistic effect of **POMOF-1**, a series of control experiments were carried out by employing the precursors of **POMOF-1** and their mixtures as catalysts (Table 3). The catalytic result demonstrated that NHPI itself can promote the oxidation but with a low yield of 53% for **2a** (Table 3, entry 2). Using CuCl₂ or {CrMo₆} as catalyst, each can enhance the conversion of toluene up to 70% as compared with NHPI alone (Table 3, entries 3 and 4). However, the adduct (**3**) of benzoic acid and NHPI was obtained as side product in the yield of 26%

for CuCl$_2$ (Table 3, entry 3). On the contrary, utilization of **L** together with NHPI resulted in dramatic decrease of the yield (Table 3, entry 5). In view of the binary mixtures of the precursors, **3** was always observed in the presence of CuCl$_2$ while the yield of **2a** is generally lower than that of NHPI when the mixtures contained **L** (Table 3, entry 6–8). In the case of tertiary mixture of CuCl$_2$ + **L** + {CrMo$_6$}, the overall yield is 64% with a ratio of 47/17 for **2a/3** (Table 3, entry 9). In summary, the control experiments ambiguously demonstrated the synergistic effect from the rational assembly of multiple components of **POMOF-1**, which not only furnished the best yield of **2a** but also avoided the formation of **3**.

Catalytic oxidation of alkylarenes by POMOF-1

Encouraged by the successful oxidation of methylarenes, we try to use **POMOF-1** to study the oxidation reaction of other alkylarenes. The catalysis was probed with ethylbenzene (**4a**) as a model substrate (Table S2†). Adopting the same conditions as oxidation of methylarenes, acetophenone (**5a**) was afforded in high yield of 91% (Table S2,† entry 1). Reduction of the reaction time from 24 h to 6 h, **5a** can also be obtained in a yield of 90% (Table S2,† entry 3). The subsequent screening of the amount of NHPI, reaction temperature and solvents indicated that the best yield can be achieved by performing the reaction at 85 °C in CH$_3$CN with 0.2 equivalent of NHPI as co-catalyst (Table S2,† entries 4–11). By combination of 1 mol% **POMOF-1** and the reaction time of 6 h, the optical conditions are thus established (Table S2,† entry 3).
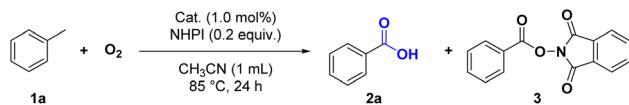
After determining the optical conditions (Table S2,† entry 3), the general applicability for oxidation reaction of alkylarenes was then investigated. As shown in Table 4, the reaction showed good functional group tolerance for ethyl benzene derivatives. Ethyl benzenes containing both electron-donating and electron-withdrawing substituents can be efficiently converted into corresponding ketones in excellent yields ranging from 85% to 93%

(**5b–5f**). Extending alkyl group from ethyl to propyl and cyclo-alkane, **5g** and **5h** were afforded in 80% and 70% yields, respectively. The catalytic system was also tolerant with substrate bearing bulky substituent on aromatic ring, 4-phenylethyl benzene was converted to **5i** in a good yield of 86%. The method can be facilely extended to substrates containing arylmethylene groups, the oxidation of diphenylmethane and fluorene proceeded smoothly to give **5j–5l** in good yields. When unsymmetrically substituted 4-methyl ethylbenzene was subjected to the oxidation, **5m** could be afforded in high yield of 95%, indicating that the oxidation preferred to occur on the secondary C–H bond. As expected, the oxidation of tertiary C–H bond can only result in alcohol **5n** as the sole product. Similar to the oxidation of methylarenes, control experiments also demonstrated the synergistic effect of **POMOF-1** during catalysis, which exhibited remarkably improved activity than the precursors or the mixture of the individual components (Table S3†).

Recyclability and heterogeneity of POMOF-1

To test the recyclability and stability of **POMOF-1**, it was reused for 5 cycles towards oxidation of toluene and ethylbenzene, respectively. In each case, the catalytic activity was maintained without appreciable loss (Fig. S5†). The PXRD patterns and FT-IR spectra of the recovered catalysts matched well with pristine sample, indicative of the preservation of structural integrity (Fig. S6 and S7†). Moreover, ICP analysis of **POMOF-1** before and after catalysis showed little change, further confirming the structural stability of **POMOF-1** (Table S4†). Additionally, ICP analysis of the filtered solution after catalysis indicated negligible amounts of metal ions (<0.01%), demonstrating no leaking of catalyst and heterogeneous nature during the reaction
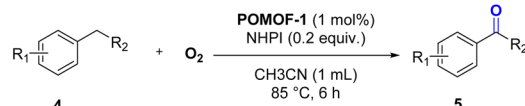
Table 3 Control experiments for oxidation reaction of toluene (**1a**)^a

Entry	Cat.	**2a** yield%	**3** yield%
1	**POMOF-1**	91	Trace
2	None	53	Trace
3	CuCl$_2$	44	26
4	{CrMo$_6$}	75	Trace
5	**L**	23	Trace
6	CuCl$_2$ + **L**	32	20
7	CuCl$_2$ + {CrMo$_6$}	51	17
8	{CrMo$_6$} + **L**	45	Trace
9	CuCl$_2$ + **L** + {CrMo$_6$}	47	17

^{a} Reaction condition: cat. (1 mol%), NHPI (0.2 equiv.), toluene **1a** (0.2 mmol) and CH$_3$CN (1 mL) in O$_2$ (1 atm) at 85 °C for 24 h. Yields were determined by GC-MS. Hexadecane as internal standard.

Table 4 Oxidation coupling reaction of alkylarenes^a

5a, 90% (85%) 5b, 93% (88%) 5c, 4-Br, 90% (85%); 5d, 3-Br, 87% (86%); 5e, 2-Br, 85% (81%) 5f, 86% (80%)

5g, 80% (78%) 5h, 70% (65%) 5i, 86% (81%) 5j, 85% (84%)

5k, 56% (51%) 5l, 99% (94%) 5m, 95% (91%) 5n, 99% (91%)

^{a} Reaction condition: **POMOF-1** (1 mol%), NHPI (0.2 equiv.), alkylarenes **4** (0.2 mmol) and CH$_3$CN (1 mL) in O$_2$ (1 atm) at 85 °C for 6 h. Yields were determined by GC-MS. Hexadecane as internal standard. Values in parentheses are the isolated yields.

(Table S4†). Hot filtration tests revealed the reactions didn't completely stop but proceeded in much lower conversion (Fig. S8†). This was probably caused by the catalysis of residual NHPI in the filtrate.

Mechanism study

With toluene and ethylbenzene as model substrates, a series of experiments are performed to reveal the reaction mechanisms for oxidative transformation (Scheme 2). For the oxidation of toluene, detection of the reaction mixture after 12 h by GC-MS showed both the targeted **2a** and intermediate **3** are presented in solution (Scheme 2a and Fig. S9†). Extension of the reaction time to 24 h at which point the catalysis was complete, **2a** was the sole product detected by GC-MS (Fig. S9†). This implied **2a** was probably generated by disassociation of **3**. To verify this point, **3** was synthesized and used as reactant for hydrolysis under the same conditions as oxidation of toluene. With **POMOF-1** as catalyst, **3** could be hydrolyzed to benzoic acid in 95% yield (Scheme 2b and Fig. S10†). The above results ambiguously indicated **3** was the key intermediate during catalysis, which underwent hydrolysis to produce **2a**. On the other hand, radical scavengers were introduced into the catalytic system to probe other active and intermediate species. The reaction was totally suppressed by adding 2 equiv. TEMPO, indicating that the reaction proceeded in a radical pathway
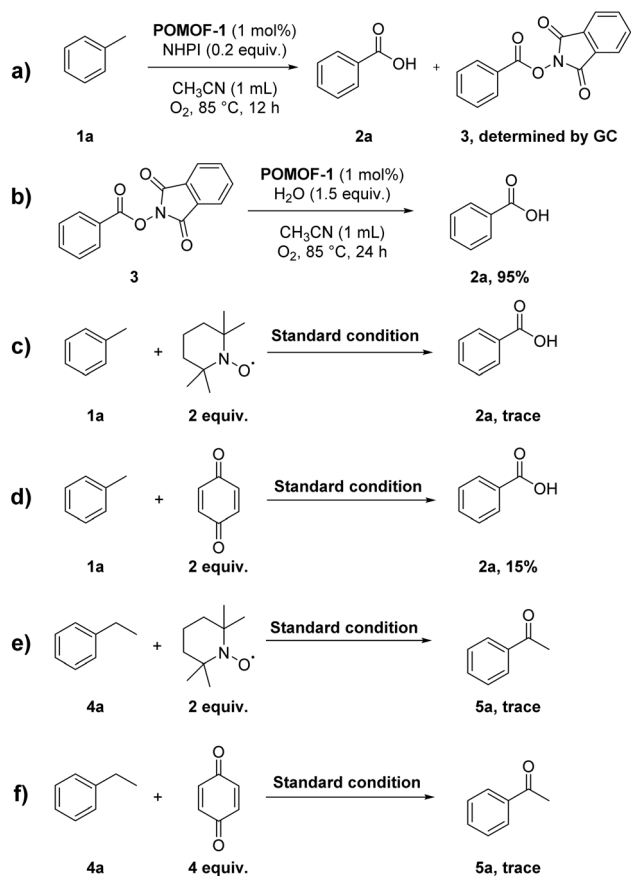

Scheme 2 Control experiments for mechanism study.
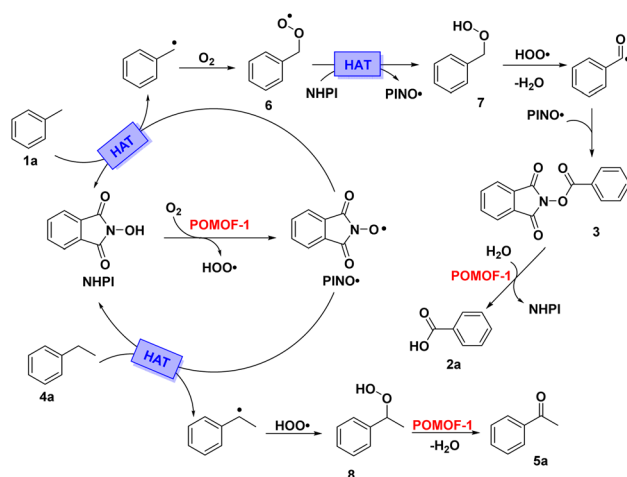
Scheme 3 Proposed mechanisms for oxidation of methylarenes and alkylarenes.

(Scheme 2c). Meanwhile, benzoquinone could suppress the reaction as well, suggesting HOO˙ was probably the active species that furnish the oxidation (Scheme 2d). Adopting the same procedure for the oxidation of ethylbenzene, both TEMPO and benzoquinone can suppress the transformation (Scheme 2e and f). Therefore, HOO˙ was proposed as the reactive oxygen species to promote the formation of ketone.

Based on the experimental results and well-established reaction pathways in literature,[61,64–66] the plausible mechanisms for catalytic oxidation of methylarenes and alkylarenes are proposed in Scheme 3. Initially, O_2 and NHPI interact with **POMOF-1** to afford HOO˙ and PINO˙. The benzylic C–H bonds of toluene and ethylbenzene are then activated by PINO˙ *via* hydrogen atom transfer (HAT) process to generate toluene radical and ethylbenzene radical, respectively. Upon oxidation by O_2, the toluene radical is converted into intermediate **6**. Afterwards, **6** undergoes HAT with NHPI to produce **7**, which is further oxidized by HOO˙ and then coupled with PINO˙ to give the key intermediate **3**. Finally, **3** could be hydrolyzed by **POMOF-1** and thus give rise to benzoic acid (**2a**). In view of the ethylbenzene radical, it undergoes direct oxidation by HOO˙ to get intermediate **8**, which is then transformed to **5a** *via* the dehydration catalyzed by **POMOF-1**.

Conclusion

In conclusion, we demonstrate that the self-assembly of a 2D **POMOF-1** consisted of orderly distributed Anderson-type {CrMo₆} clusters and Cu²⁺ centers for catalytic oxidation of benzylic C–H bonds to functional carbonyl groups. Coupled with NHPI as co-catalyst, **POMOF-1** efficiently promote the oxidative conversion of methylarenes and alkylarenes into aryl carboxylic acids and aromatic ketones, respectively. The high efficiency is ascribed to the synergistic effect derived from the rational combination of multiple functional components in **POMOF-1** and the cooperative catalysis with NHPI on the confined surface of **POMOF-1**. The catalyst is robust and can be

reused for five cycles with little loss of activity while maintaining the structural integrity. Mechanism study reveals that **POMOF-1** works together with NHPI to activate the benzylic C–H bonds of substrates, which are sequentially oxidized by oxygen and HOO$^\cdot$ and resulted in targeted carboxylic acids or ketones. This work manifests that combination of multifunctional POM-based frameworks with NHPI proves to be an efficient way for challenging C–H bond oxidation under mild condition, which can further promote the development of high-performance catalytic systems for advanced oxidation.

Conflicts of interest

There are no conflicts to declare.

Acknowledgements

Notes and references

1 J. H. Teles, I. Hermans, G. Franz and R. A. Sheldon, in *Ullmann's Encyclopedia of Industrial Chemistry*, Wiley-VCH, Weinheim, 2015, pp. 1–103.

2 S. Caron, R. W. Dugger, S. G. Ruggeri, J. A. Ragan and D. H. B. Ripin, Large-scale oxidations in the pharmaceutical industry, *Chem. Rev.*, 2006, **106**, 2943–2989.

3 T. Newhouse and P. S. Baran, If C-H bonds could talk: selective C-H bond oxidation, *Angew. Chem., Int. Ed.*, 2011, **50**, 3362–3374.

4 L. Kesavan, R. Tiruvalam, M. H. A. Rahim, M. I. bin Saiman, D. I. Enache, R. L. Jenkins, N. Dimitratos, J. A. Lopez-Sanchez, S. H. Taylor, D. W. Knight, C. J. Kiely and G. J. Hutchings, Solvent-free oxidation of primary carbon-hydrogen bonds in toluene using Au-Pd alloy nanoparticles, *Science*, 2011, **331**, 195–199.

5 H. Sterckx, B. Morel and B. U. W. Maes, Catalytic aerobic oxidation of C(sp3)−H bonds, *Angew. Chem., Int. Ed.*, 2019, **58**, 7946–7970.

6 J. Piera and J.-E. Bäckvall, Catalytic oxidation of organic substrates by molecular oxygen and hydrogen peroxide by multistep electron transfer—a biomimetic approach, *Angew. Chem., Int. Ed.*, 2008, **47**, 3506–3523.

7 Z. Shi, C. Zhang, C. Tang and N. Jiao, Recent advances in transition-metal catalyzed reactions using molecular oxygen as the oxidant, *Chem. Soc. Rev.*, 2012, **41**, 3381–3430.

8 Z. Guo, B. Liu, Q. Zhang, W. Deng, Y. Wang and Y. Yang, Recent advances in heterogeneous selective oxidation catalysis for sustainable chemistry, *Chem. Soc. Rev.*, 2014, **43**, 3480–3524.

9 M. Liu and C.-J. Li, in *Green Oxidation in Organic Synthesis*, Wiley-VCH, 2019, pp. 159–180.

10 H. Gu, X. Liu, X. Liu, C. Ling, K. Wei, G. Zhan, Y. Guo and L. Zhang, Adjacent single-atom irons boosting molecular oxygen activation on MnO2, *Nat. Commun.*, 2021, **12**, 5422.

11 S. Li, N. Li, G. Li, Y. Ma, M. Huang, Q. Xia, Q. Zhao and X. Chen, Silver-modified polyniobotungstate for the visible light-induced simultaneous cleavage of C–C and C–N bonds, *Polyoxometalates*, 2023, **2**, 9140024.

12 W. Partenheimer, Methodology and scope of metal/bromide autoxidation of hydrocarbons, *Catal. Today*, 1995, **23**, 69–158.

13 S. A. Chavan, S. B. Halligudi, D. Srinivas and P. Ratnasamy, Formation and role of cobalt and manganese cluster complexes in the oxidation of p-xylene, *J. Mol. Catal. A: Chem.*, 2000, **161**, 49–64.

14 W. Partenheimer, The structure of metal/bromide catalysts in acetic acid/water mixtures and its significance in autoxidation, *J. Mol. Catal. A: Chem.*, 2001, **174**, 29–33.

15 W. Partenheimer, The high yield synthesis of benzaldehydes from benzylic alcohols using homogeneously catalyzed aerobic oxidation in acetic acid, *Adv. Synth. Catal.*, 2006, **348**, 559–568.

16 R. A. F. Tomás, J. C. M. Bordado and J. F. P. Gomes, p-Xylene oxidation to terephthalic acid: a literature review oriented toward process optimization and development, *Chem. Rev.*, 2013, **113**, 7421–7469.

17 D. Lisicki, A. Maciej and B. Orlińska, Selective aerobic oxidation of toluene in the presence of Co2+ and task-specific organic salts, including ionic liquids, *Ind. Eng. Chem. Res.*, 2021, **60**, 11579–11589.

18 Y. Yoshino, Y. Hayashi, T. Iwahama, S. Sakaguchi and Y. Ishii, Catalytic oxidation of alkylbenzenes with molecular oxygen under normal pressure and temperature by N-hydroxyphthalimide combined with Co(OAc)2, *J. Org. Chem.*, 1997, **62**, 6810–6813.

19 N. Sawatari, S. Sakaguchi and Y. Ishii, Oxidation of nitrotoluenes with air using N-hydroxyphthalimide analogues as key catalysts, *Tetrahedron Lett.*, 2003, **44**, 2053–2056.

20 R. A. Sheldon and I. W. C. E. Arends, Organocatalytic oxidations mediated by nitroxyl radicals, *Adv. Synth. Catal.*, 2004, **346**, 1051–1071.

21 F. Recupero and C. Punta, Free radical functionalization of organic compounds catalyzed by N-hydroxyphthalimide, *Chem. Rev.*, 2007, **107**, 3800–3842.

22 M. Caruso, S. Navalón, M. Cametti, A. Dhakshinamoorthy, C. Punta and H. García, Challenges and opportunities for N-hydroxyphthalimide supported over heterogeneous

solids for aerobic oxidations, *Coord. Chem. Rev.*, 2023, **486**, 215141.

23 I. K. Goncharova, K. P. Silaeva, A. V. Arzumanyan, A. A. Anisimov, S. A. Milenin, R. A. Novikov, P. N. Solyev, Y. V. Tkachev, A. D. Volodin, A. A. Korlyukov and A. M. Muzafarov, Aerobic Co-/N-hydroxysuccinimide-catalyzed oxidation of p-tolylsiloxanes to p-carboxyphenylsiloxanes: synthesis of functionalized siloxanes as promising building blocks for siloxane-based materials, *J. Am. Chem. Soc.*, 2019, **141**, 2143–2151.

24 B. Dutta, R. Clarke, S. Raman, T. D. Shaffer, L. Achola, P. Nandi and S. L. Suib, Lithium promoted mesoporous manganese oxide catalyzed oxidation of allyl ethers, *Nat. Commun.*, 2019, **10**, 655.

25 X. Huang, G. Lu, K. Zhang, J. Liu, H. Zhang, Z. Guo and J. Tao, Selective synthesis of imines by direct oxidative coupling of amines on Cu-doped CeO2 catalysts, *Appl. Surf. Sci.*, 2020, **514**, 145948.

26 C. Zhang, Z. Huang, J. Lu, N. Luo and F. Wang, Generation and confinement of long-lived N-oxyl radical and its photocatalysis, *J. Am. Chem. Soc.*, 2018, **140**, 2032–2035.

27 R. Ma, W. Chen, L. Wang, X. Yi, Y. Xiao, X. Gao, J. Zhang, X. Tang, C. Yang, X. Meng, A. Zheng and F.-S. Xiao, N-oxyl radicals trapped on Zeolite surface accelerate photocatalysis, *ACS Catal.*, 2019, **9**, 10448–10453.

28 A. Dhakshinamoorthy, A. M. Asiri and H. Garcia, Metal–organic frameworks as catalysts for oxidation reactions, *Chem.–Eur. J.*, 2016, **22**, 8012–8024.

29 A. Dhakshinamoorthy, M. Alvaro and H. Garcia, Aerobic oxidation of benzyl amines to benzyl imines catalyzed by metal–organic framework solids, *ChemCatChem*, 2010, **2**, 1438–1443.

30 A. Dhakshinamoorthy, M. Alvaro and H. Garcia, Aerobic oxidation of cycloalkenes catalyzed by iron metal organic framework containing N-hydroxyphthalimide, *J. Catal.*, 2012, **289**, 259–265.

31 A. Dhakshinamoorthy, M. Alvaro and H. Garcia, Atmospheric-pressure, liquid-phase, selective aerobic oxidation of alkanes catalysed by metal–organic frameworks, *Chem.–Eur. J.*, 2011, **17**, 6256–6262.

32 Y. Wang, L. Zhao, S. Liu, G. Ji, C. He, Y. Tang and C. Duan, Mixed-component metal–organic framework for boosting synergistic photoactivation of C(sp3)–H and oxygen, *ACS Appl. Mater. Interfaces*, 2023, **15**, 16744–16754.

33 D.-L. Long, R. Tsunashima and L. Cronin, Polyoxometalates: building blocks for functional nanoscale systems, *Angew. Chem., Int. Ed.*, 2010, **49**, 1736–1758.

34 H. N. Miras, J. Yan, D.-L. Long and L. Cronin, Engineering polyoxometalates with emergent properties, *Chem. Soc. Rev.*, 2012, **41**, 7403–7430.

35 H. N. Miras, L. Vilà-Nadal and L. Cronin, Polyoxometalate based open-frameworks (POM-OFs), *Chem. Soc. Rev.*, 2014, **43**, 5679–5699.

36 S.-S. Wang and G.-Y. Yang, Recent advances in polyoxometalate-catalyzed reactions, *Chem. Rev.*, 2015, **115**, 4893–4962.

37 A. Bijelic, M. Aureliano and A. Rompel, Polyoxometalates as potential next-generation metallodrugs in the combat against cancer, *Angew. Chem., Int. Ed.*, 2019, **58**, 2980–2999.

38 M. R. Horn, A. Singh, S. Alomari, S. Goberna-Ferrón, R. Benages-Vilau, N. Chodankar, N. Motta, K. Ostrikov, J. MacLeod, P. Sonar, P. Gomez-Romero and D. Dubal, Polyoxometalates (POMs): from electroactive clusters to energy materials, *Energy Environ. Sci.*, 2021, **14**, 1652–1700.

39 I. A. Weinstock, R. E. Schreiber and R. Neumann, Dioxygen in polyoxometalate mediated reactions, *Chem. Rev.*, 2018, **118**, 2680–2717.

40 N. Mizuno and K. Kamata, Catalytic oxidation of hydrocarbons with hydrogen peroxide by vanadium-based polyoxometalates, *Coord. Chem. Rev.*, 2011, **255**, 2358–2370.

41 X. Chen, G. Zhang, B. Li and L. Wu, An integrated giant polyoxometalate complex for photothermally enhanced catalytic oxidation, *Sci. Adv.*, 2021, **7**, eabf8413.

42 J. Liu, N. Jiang, J.-M. Lin, Z.-B. Mei, L.-Z. Dong, Y. Kuang, J.-J. Liu, S.-J. Yao, S.-L. Li and Y.-Q. Lan, Structural evolution of giant polyoxometalate: from "Keplerate" to "Lantern" type Mo132 for improved oxidation catalysis, *Angew. Chem., Int. Ed.*, 2023, **62**, e202304728.

43 J. Song, M. Hua, X. Huang, J. Ma, C. Xie and B. Han, Robust bio-derived polyoxometalate hybrid for selective aerobic oxidation of benzylic C(sp3)–H bonds, *ACS Catal.*, 2023, **13**, 4142–4154.

44 J. Li, D. Zhang, Y. Chi and C. Hu, Catalytic application of polyoxovanadates in the selective oxidation of organic molecules, *Polyoxometalates*, 2022, **1**, 9140012.

45 A. Khoshyan, M. Pourtahmasb, F. Feizpour, M. Jafarpour and A. Rezaeifard, Aerobic {Mo72V30} nanocluster-catalysed heterogeneous one-pot tandem synthesis of benzimidazoles, *Appl. Organomet. Chem.*, 2019, **33**, e4638.

46 A. Rezaeifard, A. Khoshyan, M. Jafarpour and M. Pourtahmasb, Selective aerobic benzylic C–H oxidation co-catalyzed by N-hydroxyphthalimide and Keplerate {Mo72V30} nanocluster, *RSC Adv.*, 2017, **7**, 15754–15761.

47 M. Zhao, X.-W. Zhang and C.-D. Wu, Structural transformation of porous polyoxometalate frameworks and highly efficient biomimetic aerobic oxidation of aliphatic alcohols, *ACS Catal.*, 2017, **7**, 6573–6580.

48 M. Zhao and C.-D. Wu, Biomimetic activation of molecular oxygen with a combined metalloporphyrinic framework and co-catalyst platform, *ChemCatChem*, 2017, **9**, 1192–1196.

49 P. Wu, P. Yin, J. Zhang, J. Hao, Z. Xiao and Y. Wei, Single-side organically functionalized Anderson-type polyoxometalates, *Chem.–Eur. J.*, 2011, **17**, 12002–12005.

50 X.-X. Li, X. Ma, W.-X. Zheng, Y.-J. Qi, S.-T. Zheng and G.-Y. Yang, Composite hybrid cluster built from the integration of polyoxometalate and a metal halide cluster: synthetic strategy, structure, and properties, *Inorg. Chem.*, 2016, **55**, 8257–8259.

51 X. Wang, Z. Chang, H. Lin, A. Tian, G. Liu and J. Zhang, Assembly and photocatalysis of two novel 3D Anderson-type polyoxometalate-based metal–organic frameworks constructed from isomeric bis(pyridylformyl)piperazine ligands, *Dalton Trans.*, 2014, **43**, 12272–12278.
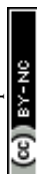
52 X. Wang, Z. Chang, H. Lin, A. Tian, G. Liu, J. Zhang and D. Liu, Two novel Anderson-type polyoxometalate-based metal–organic complexes with high-efficiency photocatalysis towards degradation of organic dyes under UV and visible light irradiation, *RSC Adv.*, 2015, **5**, 14020–14026.

53 J. Zhang, Y. Huang, G. Li and Y. Wei, Recent advances in alkoxylation chemistry of polyoxometalates: from synthetic strategies, structural overviews to functional applications, *Coord. Chem. Rev.*, 2019, **378**, 395–414.

54 H. Yu, S. Ru, G. Dai, Y. Zhai, H. Lin, S. Han and Y. Wei, An efficient iron(III)-catalyzed aerobic oxidation of aldehydes in water for the green preparation of carboxylic acids, *Angew. Chem., Int. Ed.*, 2017, **56**, 3867–3871.

55 Z. Wei, J. Wang, H. Yu, S. Han and Y. Wei, Recent advances of Anderson-type polyoxometalates as catalysts largely for oxidative transformations of organic molecules, *Molecules*, 2022, **27**, 5212.

56 J. Wang, H. Yu, Z. Wei, Q. Li, W. Xuan and Y. Wei, Additive-Mediated Selective Oxidation of Alcohols to Esters via Synergistic Effect Using Single Cation Cobalt Catalyst Stabilized with Inorganic Ligand, *Research*, 2020, **2020**, 3875920.

57 C. P. Delaney, E. Lin, Q. Huang, I. F. Yu, G. Rao, L. Tao, A. Jed, S. M. Fantasia, K. A. Püntener, R. D. Britt and J. F. Hartwig, Cross-coupling by a noncanonical mechanism involving the addition of aryl halide to Cu(II), *Science*, 2023, **381**, 1079–1085.

58 S. Bhunia, G. G. Pawar, S. V. Kumar, Y. Jiang and D. Ma, Selected copper-based reactions for C−N, C−O, C−S, and C−C bond formation, *Angew. Chem., Int. Ed.*, 2017, **56**, 16136–16179.

59 S. Nakai, T. Yatabe, K. Suzuki, Y. Sasano, Y. Iwabuchi, J.-y. Hasegawa, N. Mizuno and K. Yamaguchi, Methyl-selective α-oxygenation of tertiary amines to formamides by employing copper/moderately hindered nitroxyl radical (DMN-AZADO or 1-Me-AZADO), *Angew. Chem., Int. Ed.*, 2019, **58**, 16651–16659.

60 R. Trammell, K. Rajabimoghadam and I. Garcia-Bosch, Copper-promoted functionalization of organic molecules: from biologically relevant Cu/O2 model systems to organometallic transformations, *Chem. Rev.*, 2019, **119**, 2954–3031.

61 H. Chen, L. Wang, S. Xu, X. Liu, Q. He, L. Song and H. Ji, Selective functionalization of hydrocarbons using a ppm bioinspired molecular tweezer via proton-coupled electron transfer, *ACS Catal.*, 2021, **11**, 6810–6815.

62 C. Hansch, A. Leo and R. W. Taft, A survey of Hammett substituent constants and resonance and field parameters, *Chem. Rev.*, 1991, **91**, 165–195.

63 G. A. DiLabio, P. Franchi, O. Lanzalunga, A. Lapi, F. Lucarini, M. Lucarini, M. Mazzonna, V. K. Prasad and B. Ticconi, Hydrogen atom transfer (HAT) processes promoted by the quinolinimide-N-oxyl radical. A kinetic and theoretical study, *J. Org. Chem.*, 2017, **82**, 6133–6141.

64 M. A. Hoque, J. Twilton, J. Zhu, M. D. Graaf, K. C. Harper, E. Tuca, G. A. DiLabio and S. S. Stahl, Electrochemical PINOylation of methylarenes: improving the scope and utility of benzylic oxidation through mediated electrolysis, *J. Am. Chem. Soc.*, 2022, **144**, 15295–15302.

65 P. Li, J. Sun, X. Xu, Z. Mi, Y. Lin, J. Cheng, R. Bai and Y. Xie, Ferric nitrate-promoted oxidative esterification of toluene with N-hydroxyphthalimide: synthesis of N-hydroxyimide esters, *Tetrahedron Lett.*, 2018, **59**, 2640–2643.

66 K. Singha, S. C. Ghosh and A. B. Panda, Visible light-driven efficient synthesis of amides from alcohols using Cu−N−TiO2 heterogeneous photocatalyst, *Eur. J. Org Chem.*, 2021, **2021**, 657–662.